Local Dynamics of Polyethylene and Its Oligomers: A Molecular Dynamics Interpretation of the Incoherent Dynamic Structure Factor

G. Arialdi, K. Karatasos,‡ and J.-P. Ryckaert*

Laboratoire de Physique des Polymères, CP 223, Université Libre de Bruxelles, Bd du Triomphe, B-1050 Brussels, Belgium

V. Arrighi and F. Saggio

Chemistry Department, Heriot-Watt University, Edinburgh, EH14 4AS, UK

A. Triolo,† A. Desmedt,§ J. Pieper, and R. E. Lechner

Hahn-Meitner-Institut/BENSC, Glienicker Strasse 100, D-14109 Berlin, Germany

Received September 16, 2002; Revised Manuscript Received August 12, 2003

ABSTRACT: We present a detailed study of the local dynamics of short polyethylene (PE) chains using molecular dynamics (MD) simulations and quasi-elastic neutron scattering (QENS) data. QENS measurements were carried out on two samples having different chain lengths: $C_{44}H_{90}$ and PE2K (M_w = 2150 g/mol). The incoherent dynamic structure factors obtained from experiments at $T = 450$ K and MD simulations carried out at the same temperature are compared in the range $0.5 \leq Q \leq 2.0$ Å^{-1}. Agreement between experimental data and simulations is quantitative. Attempts are made to characterize the momentum transfer and the chain length dependence of the $I(Q,t)$ and $S(Q,\omega)$ data on the basis of the Kohlrausch−Williams−Watts (KWW) function and two exponentials relaxation functions in time. As MD simulation data cover a broader frequency window and have a very low statistical noise, a more refined analysis of the intermediate scattering functions in terms of a continuous linear combination of exponentials weighted by a distribution of relaxation times has been performed. This analysis shows a systematic evolution of the shape of the distribution of relaxation times going from a two-process situation at low Q toward a single merged process at higher Q. This allows us to point out in a well-defined case the limitations of both the KWW and two exponentials descriptions which approximate the distribution of relaxation times either as one broad and asymmetric distribution or as a conjunction of two delta distributions.

I. Introduction

The local dynamics of polyethylene (PE) has been investigated over many years using both experiments (e.g., rheology,[1−3] NMR,[4] etc.) and simulations.[5−13] A number of neutron scattering studies have been carried out on this polymer,[12−20] some of these dealing with experiments below the melting temperature, T_m.[14−17] One of the first quasi-elastic neutron scattering (QENS) experiments on polyethylene melts was reported by Rennie et al.,[18] who investigated the diffusion of relatively short protonated molecules ($C_{36}H_{74}$ and $C_{40}H_{82}$) in a deuterated polyethylene matrix. These measurements were confined to the low Q region and were limited to a relatively narrow energy transfer range (−1 to 10 μeV). While high molecular weight PE has been studied by QENS,[17,20] there is a lack of experimental data on short PE chains, which can be directly compared to the results that are becoming available from simulations. To date, only one neutron study of local dynamics in a long-chain alkane, n-$C_{100}H_{202}$, at 504 K has been reported in the literature.[12] In that work a detailed comparison between experimental QENS data and molecular dynamics (MD) simulations is given, but this is restricted to the Q dependence of the intermediate scattering function of n-$C_{100}H_{202}$ at a single temperature.

This latter study[12] established that, in the momentum transfer Q range above 0.5 Å^{-1}, the incoherent generalized susceptibility $\omega S(Q,\omega)$ shows a single broad peak in frequency, indicating that the local dynamics relaxation in PE at 504 K proceeds via a single process. The latter was interpreted as a composite process resulting from the combination of torsion oscillations and conformational jumps leading, on the local scale, to relaxation effects taking place on similar time scales. This is in contrast with the situation of many polymer melts (e.g., polyisoprene,[21] poly(vinyl chloride),[22] polybutadiene,[23] and polypropylene[24]) at temperatures not too far above T_g where a fast process (occurring within a picosecond) due for a large part to torsion oscillations of the backbone and a slower diffusive process related to conformational jumps are found to be very well-resolved in time. In these polymers, the $I(Q,t)$ relaxation has been related to the well-known two-step decay characteristic of glass-forming supercooled liquids. Attempts to interpret the incoherent dynamic structure factor of PE in a slightly lower temperature regime on the basis of two separate processes can be found in the neutron scattering studies of Buchenau et al.[19] and Kanaya et al.[20]

Our present study aims to assess to what extent, in PE melts, it is possible to unravel two dynamic processes in the local dynamics relaxation. We highlight methods

* To whom correspondence should be addressed.
† Present address: CNR, Via La Farina 237, 98123 Messina, Italy.
‡ Present address: Dept. Chem. Eng., PO Box 420, 54114, Thessaloniki, Greece.
§ Present address: Lab. de Phys.-Chim. Moléculaire, UMR5803 CNRS-Univ. de Bordeaux I, 351 cours de la Libération, 33405 Talence, France.

10.1021/ma0256789 CCC: $25.00
Published on Web 10/22/2003

that can be used to appreciate the Q and temperature dependences which are a first step toward their detailed characterization. More generally, this work extends the direct comparison between quasi-elastic neutron scattering and MD computer simulations to a lower temperature regime ($T = 450$ K) with respect to former studies[12] and discusses some aspects of the molar mass dependence of PE local chain dynamics. This is the first paper of a series where we describe a systematic analysis of the local dynamics of PE in terms of molecularly interpreted processes. In the present paper, we discuss new QENS and MD results on samples with chain lengths in the range $C_{44}-C_{154}$ at 450 K in a Q range going from 0.5 up to 2.0 Å^{-1}. The largest chain length sample is widely known as "PE2K" for its approximately 2000 Da molar mass.

Section II discusses technical details associated with the time-of-flight experiments and samples. Section III is devoted to a description of the atomistic model used in simulations and the type of computer experiments which were conducted. As our molecular dynamics simulations are dealing with a single polydisperse PE sample, we explain how the local dynamics relaxation data on C_{44} and PE2K has been estimated from the data and why the polydisperse nature of the sample was found to be useful. Section IV is devoted to the direct comparison for both chain lengths at various Q values, between the experimental incoherent dynamic structure factor and its prediction from simulations. To simplify notations, the incoherent dynamic structure factor will be denoted $S(Q,\omega)$ and the corresponding intermediate scattering function $I(Q,t)$, given the absence of ambiguity with any coherent signal. We will however distinguish $S(Q,\omega)$ from its version convoluted with the experimental resolution function, which will be written as $S^c(Q,\omega)$. In section V, we first parametrize the intermediate scattering function with a stretched exponential. This choice is guided by the versatility of this function to represent a complex relaxation process which is intrinsically, as discussed above, a composite one. Initially, such a fit is attempted on the experimental and simulation data, as restricted to the accessible experimental frequency window, i.e., at most -1 to 10 meV. Exploiting then the larger frequency window offered by 12 ns long MD simulations, we use the same functional form to fit the complete relaxation curves. With this two-parameter description which turns out to represent data adequately in the experimentally accessible window, the various aspects of our study (chain size, Q dependence, resolution effects) can be discussed in terms of a minimal set of parameters. In a second step, we report an attempt to represent the same experimental and simulated relaxation functions (for PE2K) by a sum of two Lorentzians and we explore the nature of the composite process and the possibility to unravel its two components within the probed Q regime and accessible frequency window. This last discussion prepares for the section VI where a distribution of relaxation times analysis is performed on the simulation data, exploiting the accessible wide time window which allows to follow the whole relaxation (up to the point it vanishes). This approach offers a better understanding on the Q dependence of the relaxation function as it indicates the trend from a unimodal distribution of relaxation times at high Q toward a bimodal structure at larger length scales. Section VII summarizes and concludes our findings. Further aspects on the temperature dependence of the PE local dynamics are presented in another paper.[25]

II. Materials and QENS Experiments

Two polyethylene samples were used for the neutron scattering measurements: (a) PE2K, with $M_w = 2150$ g/mol ($M_w/M_n < 1.15$) from Scientific Polymer Products, and (b) normal tetratetracontane, $C_{44}H_{90}$, from Aldrich. A slab geometry was used for all measurements; sample thickness was ca. 0.18 mm, leading to a transmission of approximately 0.9. This high value ensures that multiple scattering effects are kept to a minimum.

Neutron scattering measurements were carried out at 450 K on PE2K and $C_{44}H_{90}$ using the time-of-flight spectrometer NEAT[26] at the BENSC facility in Berlin (Germany). The scattering of a vanadium sample was also measured in order to determine the Q-dependent instrumental resolution. The incident neutron wavelength was $\lambda = 5.1$ Å, giving an energy resolution of ca. 95 μeV (determined as full width at half-maximum). The incoherent dynamic structure factor was measured as a function of scattering angle in the range 13.35°−136.65°. Because of the wide energy range which is covered by the measurement, i.e. −1.0 to 10.0 meV, the $\hat{S}(\theta,\omega)$ data corresponding to the scattered intensity as a function of energy transfer at constant scattering angle, θ, cannot be simply converted to the incoherent dynamic structure factor $S(Q,\omega)$ at constant Q. For this purpose, an interpolation procedure was used (INGRID code[27]) after correcting the data in the usual way (subtraction of empty can, detector efficiency normalization using vanadium, and absorption corrections). The constant Q interpolation led to a series of Q values for elastic scattering ($Q = [4\pi/\lambda] \sin[\theta/2]$) in the range 0.37−2.26 Å^{-1}. The same constant Q interpolation was also used to obtain the incoherent dynamic structure factor at Q values that matched MD calculations, i.e., 0.5, 0.75, 1.0, 1.25, 1.5, 1.75, and 2 Å^{-1} ($\Delta Q = 0.25$ Å^{-1}). After the constant Q interpolation, the energy transfer, ΔE, range becomes Q-dependent. Maximum ΔE values vary between 1.40 and 10.0 meV for Q increasing from 0.5 to 1.5 Å^{-1}. These upper limits in energy mean that information on $S(Q,\omega)$ and $I(Q,t)$ is limited respectively by a maximum angular frequency ω_{max} or by a minimum time $t_{min} = 2\pi/\omega_{max}$, which are $\omega_{max} = 2.13 \times 10^{12}$ rad/s and $t_{min} = 2.95$ ps at $Q = 0.5$ Å^{-1} and $\omega_{max} = 1.52 \times 10^{13}$ rad/s or $t_{min} = 0.41$ ps at $Q = 1.5$ Å^{-1}. Values of t_{max}, the longest time for which we have information, are determined by the instrumental resolution and, for all Q values, are effectively of the order of 20 ps. (More precisely, a Gaussian resolution function identifies the resolution time with $\tau_{res} = \sqrt{8\ln 2}(\text{fwhm})^{-1} = 16.3$ ps.) For the purpose of subsequent data analysis, a smooth resolution function was used. This was obtained by fitting the $S(Q,\omega)$ data of a vanadium sample using a Gaussian (as main component) and a very small Lorentzian term to improve the agreement at the "foot" of the measured resolution function.

III. Simulation: Experiments and Data Treatment

a. Experiments and Strategy. Our MD simulations were performed in a way that largely mimics a former MD study of PE at 450 K by Harmandaris et al.[8] to which we refer for details. The PE united atom (UA) model and the polydisperse sample adopted in both MD studies are identical. All methyl and methylene groups are represented by Lennard-Jones units, located at the carbon nuclei, which model the nonbonded interactions (both intermolecular and intramolecular). The Ryckaert−Bellemans torsional potential[28] is employed for all dihedral angles. While C−C bond lengths are taken as rigid, harmonic bending potentials are explicitly considered. Well-equilibrated configurations were produced by a constant pressure/constant temperature Monte Carlo (MC) procedure which, together with other types of moves (reptations, end rotations, flips, and

concerted rotations), allows for end-bridging moves[29,30] which modify the connectivity of monomers within chains. The end-bridging move conserves the total number of carbon groups and the total number of chains but allows progressively a full sampling of the adopted chain length distribution. More precisely, the underlying statistical ensemble is the semigrand ensemble $[N_c n_{mon} p T \mu^*]$ where both the total number of chains ($N_c = 20$) and the total number of methylene groups ($n_{mon} = 1560$) are imposed. The number-average chain length (expressed as N for the number of skeletal carbons) is thus fixed to $\langle N \rangle_n = n_{mon}/N_c$. Other imposed external parameters are the temperature, the pressure, and a reduced chemical potential spectrum $\mu^*(N)$ which leads to a particular distribution of chain lengths within the sample.[8,29] In our study, we adopted a uniform distribution of chain lengths between C_{39} and C_{117} (giving an average $M_n = 1094$ Da, that is C_{78}). The MC generated configurations were used to obtain initial configurations for the dynamics. Instead of performing a single very long MD trajectory, we performed 10 MD trajectories of 12 ns (each of them run in constant energy and constant volume conditions) from well-equilibrated independent starting configurations characterized by the same total number of carbon groups but different chain length distributions, volumes, and energies. These initial configurations were selected from a long MC trajectory performed at $p = 1$ atm, $T = 450$ K, giving an average specific volume of 1.293 ± 0.007 cm^3/g, in agreement with the Pant and Theodorou value.[29] With respect to the experimental value,[31] this specific volume appears to be 2−4% too low.

The same polydisperse system was studied at other temperatures ($T = 504$ K and $T = 350$ K where PE remains purely amorphous in the simulation) at $p = 1$ atm using the same scheme, and additionally, a monodisperse PE2K system of 20 chains was simulated by a standard microcanonical molecular dynamics at $T = 504$ K, $p = 1$ atm. For the $T = 504$ K experiments, specific volumes were estimated from the preliminary MC equilibrium run analogous to the one performed for the polydisperse 450 K case: we found 1.344 ± 0.005 cm^3/g for the polydisperse C_{78} case at 504 K and 1.341 ± 0.005 cm^3/g for the monodisperse C_{154} case using the same types of MC moves except the end-bridging move. The average specific volume of PE at 350 K was found to be 1.200 ± 0.006 cm^3/g. Although the present paper concentrates on the data analysis at 450 K, in the following sections, we will also refer here and there to the results from the other MD runs when it is required by the context of our discussion.

The choice of a polydisperse PE sample to predict by simulation the intermediate scattering function $I(Q,t)$ requires an explanation. To a first approximation and for sufficiently long chains, the local dynamics relaxation is expected to be independent from the chain size, and within this approximation, the use of a polydisperse sample does not present major drawbacks. Actually, to compare local dynamics experimental data on C_{44} and PE2K to simulations, we have adopted a refined analysis of our simulation data in which we distinguish specific contributions from chain core and chain end scatterers. This is detailed in the next subsection (IIIb).

It must be stressed that the major reason for our strategy to deal with a polydisperse system was motivated by our need for well-equilibrated simulated samples, as produced by the MC methodology summarized above. At 450 K, the main chain Rouse time of a chain with 154 carbons like PE2K is of the order of 10 ns.[8] At the start of our study, we felt that in order to better characterize the PE local processes, it would be useful to follow the PE local dynamics down to purely amorphous undercooled thermodynamic states (rather easy to produce in simulations, especially with polydisperse sample), reaching temperatures as low as $T = 350$ K.[25] Equilibration of PE melts at such low temperatures would be very inefficient by standard MD relaxation times, and therefore, we decided to simulate the unique polydisperse system considered here at 1 atm pressure over a large temperature window.

Further considerations on the validity of the microscopic model used and on the effect of the polydispersity on the structure and dynamics within the sample can be made. First, it has been shown[30] that the predicted X-ray structure factor, probing intra- and intermolecular contributions to the radial carbon−carbon pair distribution, is in very good agreement with the experimental data. More importantly, in the present context where the emphasis is on chain dynamics, an estimate of the chain length dependence of the viscosity coefficient of PE oligomers has shown the reliability of the microscopic model.[8] In this latter work, the viscosity of a monodisperse melt of a paraffin characterized by a chain length N at 450 K was estimated from simulation data on a polydisperse sample at that temperature, using the Rouse expression of the viscosity based on the chain longest relaxation time, a quantity which can be explicitly determined either by the end-to-end vector relaxation rate or by the center-of-mass diffusion coefficient. Also, using the present MD trajectories, we have compared the ^{13}C NMR spin−lattice relaxation time T_1 to the simulation predictions, using the spectral densities associated with the second-order orientational autocorrelation function of a C−H bond.[4] We have found an agreement similar to the one obtained in an earlier comparison exploiting monodisperse simulations of UA models.[11] To mention two examples, the T_1 value at a representative ^{13}C Larmor frequency of 75 MHz for monodisperse C_{154} at 504 K is 3.3 s in our simulations against 4.2 s predicted by the Qiu and Ediger data.[4] At 450 K and for C_{44}, the same comparison gives 2.2 s for a chain modeled in our polydisperse simulations against 3.4 s experimentally.

We thus conclude that the adopted potential, being simple, reasonably realistic, and moreover rather much investigated (which facilitates the comparison with earlier studies), is a good candidate to attempt a deep analysis of the PE chains local dynamics with special emphasis on links with experimental data. A minor point to mention here is that an additional Fixman potential term was not included in our MD calculations, as done by Harmandaris et al.,[8] to compensate for the slight ensemble difference resulting from the implicit consideration of the covalent bonds as infinitely stiff springs in the MC approach while treating them as rigid holonomic constraints in the dynamical approach.[32] For chain models such as the one adopted here which combine bond constraints and restricted bending fluctuations, the constraint effect is indeed known to be marginal.[33]

b. Chain Length Influence. As suggested by the above discussion, by simulating a polydisperse sample with the adopted PE model, we have the opportunity to extract on the basis of a single simulated system,

quantitative information on the N dependence of single chain specific properties within monodisperse systems, at a given unique temperature/pressure state point. This is what we now illustrate for the incoherent intermediate scattering function.

Taking into account the dominant incoherent cross section of hydrogen nuclei, the incoherent intermediate scattering of a fully hydrogenated PE oligomer isotropic melt is given by

$$I(Q,t) = \left\langle \frac{\sin(Q|\bar{r}_H(t) - \bar{r}_H(0)|)}{Q|\bar{r}_H(t) - \bar{r}_H(0)|} \right\rangle \quad (1)$$

where $\bar{r}_H$ denotes the coordinates of a hydrogen nucleus at time t and where the orientational part of the ensemble average has been carried out. The brackets quoted on the right-hand side of eq 1 imply both a time average (over many initial times) and an average over all hydrogen nuclei in the sample. Within the high Q regime ($Q \geq 0.5$ Å^{-1}), $I(Q,t)$ probes the local dynamics of a polymer melt. When PE chains are sufficiently long to have a clear-cut time scale separation between the local relaxation times and the global chain relaxation time, all hydrogen nuclei are usually considered as dynamically equivalent and chain size independent, chain end effects being marginal. For a monodisperse melt of PE oligomers, it must be kept in mind that the hydrogen nuclei located at different positions along the chain backbones may contribute differently to the global average in eq 1 and that chain end effects may become significant. In the following, we will thus denote as $I_N(Q,t)$ the intermediate scattering function of a monodisperse PE oligomer melt C_nH_{2n+2} (we keep N subscript for chain length, so $N = n$ in the present context). We finally note that for a polydisperse melt of PE oligomers the function $I(Q,t)$ defined by eq 1 implies an average over an even larger distribution of hydrogen species, each hydrogen atom being characterized by the length of the chain to which it belongs and by its position within this chain.

Experimentally, we have access to the intermediate scattering function $I_N(Q,t)$ relative to a particular chain length, namely $C_{44}H_{90}$ ($N = 44$, monodisperse) or PE2K ($N = 154$ with a small degree of polydispersity). Let us formally rewrite $I_N(Q,t)$ in terms of a linear combination of average contributions of two subclasses of hydrogens, denoted as $I_{ends}(Q,t;N)$ and $I_{core}(Q,t;N)$, depending parametrically on N and on the thermodynamic state. $I_{ends}(Q,t;N)$ represents the average relaxation function of chain end atoms defined as the hydrogens atoms pertaining to carbon atoms located in positions 1 up to 10 at each chain extremity,[9,10,34] giving a total of 42 hydrogens per chain. The function $I_{core}(Q,t;N)$ involves the average relaxation over the remaining chain core atoms defined as the $(2N - 40)$ methylene hydrogens attached to the $(N - 20)$ interior carbons. For the considered oligomer melt, the global intermediate scattering function $I_N(Q,t)$ is thus simply rewritten as a linear combination of the two functions $I_{ends}(Q,t;N)$ and $I_{core}(Q,t;N)$, namely

$$I_N(Q,t) = [42I_{ends}(Q,t;N) + (2N - 40)I_{core}(Q,t;N)]/(2N + 2) \quad (2)$$

In our simulations, we first note that any intermediate scattering function must be evaluated from hydrogen positions $\bar{r}_H(t)$ reconstructed from the C nuclei instantaneous positions, as the chain model consists of CH_2 united atoms. Methyl group hydrogens are never included in the average as they cannot be localized unambiguously in our simulations from the carbon positions only. Their impact on $I_N(Q,t)$ is minor as it amounts to an $1/N$ effect. As stated earlier, our MD experiments at 450 K were performed on a mixture of chains with a uniform distribution of chain lengths between C_{39} and C_{117}. Any calculation of $I(Q,t)$ was based on all 10 independent MD trajectories using atomic displacements between times t_0 and $t_0 + t$ while, within each trajectory, averaging was performed over all possible time origins t_0 to minimize statistical errors.

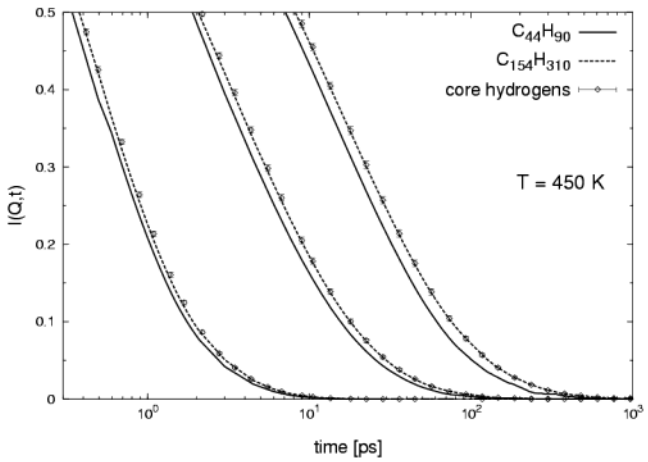

Figure 1. Comparison between the intermediate scattering functions calculated from MD simulations at 450 K as explained in the text: (a) continuous line, $I(Q,t)$ for $C_{44}H_{90}$; (b) dashed line, $I(Q,t)$ for $C_{154}H_{310}$; (c) dotted line, $I_{core}(Q,t)$ calculated after elimination of chain ends. The three data sets correspond to different Q values, i.e. 0.5, 0.75, and 1.5 Å^{-1} (in order of decreasing relaxation times).

We have estimated from these runs the chain length influence on $I_{ends}(Q,t)$ and $I_{core}(Q,t)$. To get sufficient statistics, we have computed these two functions, on the basis of the partition between end and core hydrogen atoms explained above, for three separate classes of chains within the sample: short chains with $39 \leq N \leq 49$, medium ones with $73 \leq N \leq 83$, and long chains with $107 \leq N \leq 117$. For two typical scattering vectors $Q = 0.5$ Å^{-1} and $Q = 1.5$ Å^{-1}, it is found that $I_{ends}(Q,t)$ always relaxes faster than $I_{core}(Q,t)$, the difference being of the order of 5−7%. Comparing the separate predictions for the three different classes of chain lengths, we find no significant variation of $I_{ends}(Q,t)$ or $I_{core}(Q,t)$ with N, except for the lowest $Q = 0.5$ Å^{-1} case where the short chain $I_{core}(Q,t)$ function shows a slightly faster decay than medium and longer chains, the effect being at the level of a 1% difference, just outside the statistical noise.

Given this very weak sensitivity to chain length (explored within the restricted range $39 < N < 117$) and the assumption that the local dynamics relaxation of a PE oligomer in a polydisperse melt is similar to the one affecting the same chain embedded in a monodisperse melt at the same p,T thermodynamic state, we computed the simulated $I_N(Q,t)$ curves using eq 2 with estimates of $I_{ends}(Q,t)$ and $I_{core}(Q,t)$ based on a statistics involving all chains of the sample. Figure 1 shows for various Q values at 450 K the long time decay of the intermediate scattering functions predicted for the two relevant chain lengths, namely $I_{44}(Q,t)$ and $I_{154}(Q,t)$, together with the function $I_{core}(Q,t)$, used in the $I_N(Q,t)$

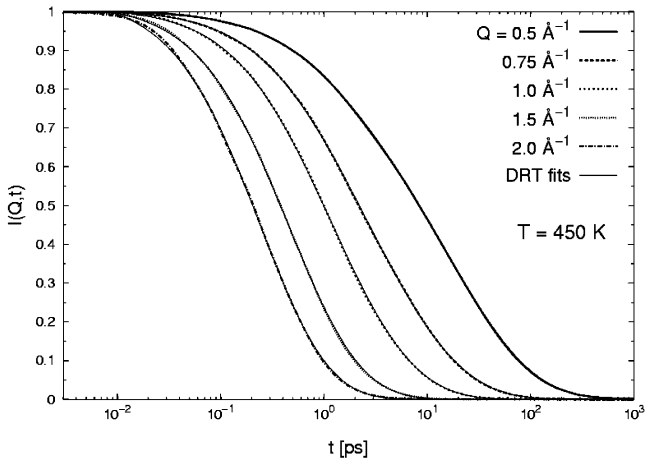

Figure 2. Incoherent intermediate structure factor $I_{core}(Q,t)$ computed by MD simulations at 450 K for $Q = 0.5$, 0.75, 1, 1.5, and 2 Å^{-1}. Thin curves are the fits resulting from the DRT analysis.

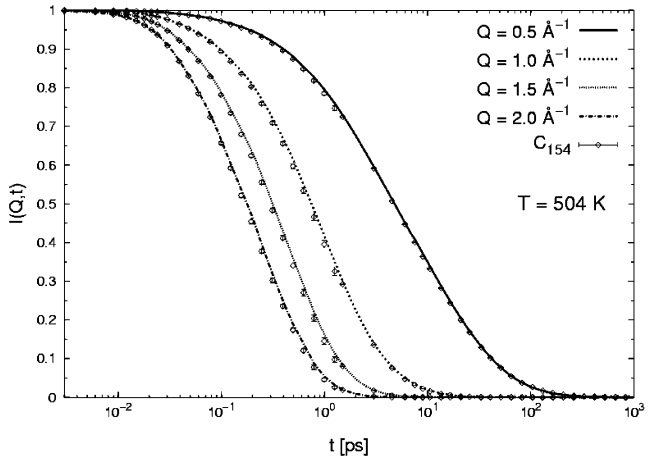

Figure 3. Intermediate scattering functions $I(Q,t)$ for PE2K simulations at 504 K, 1 atm for various Q's. The curves refer to core atoms within the polydisperse system ($\langle N\rangle_n = 78$) while the empty lozenges correspond to the core atoms in the monodisperse $C_{154}H_{310}$ sample.

estimates, which can be seen as a long chain PE prediction. This figure allows one to appreciate the importance of chain end effects on the decay of $I_N(Q,t)$ and their decrease as N increases. We indeed observe that chain end effects are becoming negligible for C_{154} given the overwhelming number of core atoms, but this is not the case for C_{44}.

The full decay of $I_{core}(Q,t)$ for Q ranging from 0.5 to 2 Å^{-1} is depicted in Figure 2. We note that, for the lowest Q value (0.5 Å^{-1}) discussed in this work, the $I(Q,t)$ function decays to a 1% level within 300 ps at 450 K. By comparison, the Rouse time of the different chains in the simulated polydisperse sample turns out to vary from $\tau_R = 600$ ps for C_{39} up to $\tau_R = 5$ ns for C_{117}.[8] This confirms the empirical observation discussed earlier that, over a time scale of 300 ps, the dynamics of hydrogen atoms which are located sufficiently far from chain ends should be independent of chain length.

We remark that the number of skeletal carbons chosen to define the chain end portion is irrelevant as long as it encompasses all atoms for which there is, on the local dynamics time scale, a significant enhanced mobility due to its position close to the chain end. This number is usually estimated to be 5 or 6.[10,34] Our strategy to reproduce $I_N(Q,t)$ from data on the polydisperse sample was tested directly at $T = 504$ K, $p =$ 1 atm, where we have both a 13.5 ns MD run of a 20-chain monodisperse $C_{154}H_{310}$ melt and a set of 10 independent 12 ns MD runs dealing with the polydisperse $C_{39}-C_{117}$ melt discussed so far in the context of 450 K data.

Figure 3 reports the $I(Q,t)$ functions obtained for the monodisperse and polydisperse systems at 504 K when only core hydrogen atoms are included in the average and we do observe that both functions agree within the statistical errors. When we include chain end contributions, the excellent agreement persists (figure not shown). This result suggests that, for polymer melts far above the glass transition, the local dynamics of a chain at fixed pressure and fixed temperature conditions is relatively insensitive to the concentration of chain ends within its environment. This property of the local dynamics for chain mixtures is in agreement with the observations of Harmandaris et al.[8] that the Rouse time τ_R of a particular chain length within an unentangled polydisperse PE melt yields a fair estimate of the rheological properties of the pure melts of chains with same size, in similar temperature and pressure conditions.

c. Calculation of the Dynamic Structure Factor $S(Q,\omega)$ and Its Convolution with the Instrumental Resolution Function. To compare time-of-flight neutron scattering data (in the present case from a single spectrometer like NEAT) and simulation predictions, we have the option either to transform experimental data from the frequency to the time domain and compare intermediate scattering functions $I(Q,t)$ or, alternatively, transform $I(Q,t)$ simulation data to the frequency domain to perform the comparison in terms of the dynamic structure factor $S(Q,\omega)$. As shown in Figure 2, for the Q range of interest and $T = 450$ K, all $I(Q,t)$ functions obtained by simulation decay to zero within the observation time (about 10 ns). The 4−5 orders of magnitude between the shortest characteristic time considered in our model (a period of the librational motion) and the longest time accessible, in combination with the very low statistical noise and the fine time grid discretization of the simulated $I(Q,t)$ data, make it more advantageous to numerically manipulate simulation data for comparison with the bare experimental data.

These numerical transformations are made robust by exploiting a very general fit of the MD $I(Q,t)$ curves in terms of a continuous linear combination of decaying exponentials

$$I(Q,t) = \int_{-\infty}^{+\infty} \mathrm{d}\ln\tau\, F(\ln\tau;Q)\exp(-t/\tau) \qquad (3)$$

where the weight $F(\ln\tau;Q)$ (normalized in the logarithmic scale) is known as the distribution of relaxation times (DRT).[9,35−37] Equation 3 shows that the $F(\ln\tau;Q)$ function is the inverse Laplace transform of the observed time correlation function. More details on the properties of $F(\ln\tau;Q)$ and its generation by the CONTIN algorithm[36,37] from an input $I(Q,t)$ function are provided in the Appendix.

Figure 2 shows the quality of the DRT fits for the core atoms dynamics in the experimental Q range. We postpone the analysis of the underlying $F(\ln\tau;Q)$ functions to section VI as, at this stage, our aim is to test the level of agreement between experimental and simu-

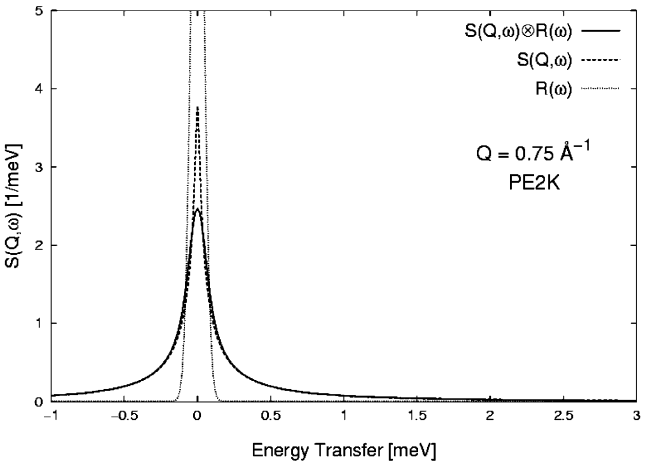

Figure 4. PE2K simulated dynamical structure factor $S(Q,\omega)$ and $S^c(Q,\omega)$, the latter being result of the convolution with the experimental resolution function $R(\omega)$, for $Q = 0.75$ Å^{-1}. The (normalized) resolution function is shown to appreciate the quasi-elastic signal broadening.

lation data and the DRT representation is used here to ease the numerical procedure. It follows from the Fourier transform of eq 3 that the dynamic structure factor $S(Q,\omega)$ can be calculated as a linear combination of Lorentzian functions

$$S(Q,\omega) = \int_{-\infty}^{+\infty} \mathrm{d}\ln\tau\, F(\ln\tau;Q)\frac{\tau}{1+(\omega\tau)^2} \qquad (4)$$

where the DRT weighting is taken from the $I(Q,t)$ fit. The resulting functions are shown in Figure 4 for $Q = 0.75$ Å^{-1}. It must be noted (see Figure 2) that the fits of $I(Q,t)$ are extremely accurate except at very short times ($t < 0.03$ ps) where the discrepancy between data and fits can be up to 1%. This effect is due to the fact that one tries to describe the short time decay of an even function having a continuous first derivative (implying a zero slope at $t = 0$) by a sum of decaying exponentials with strictly negative slope. This numerical problem is of no practical consequence as its influence on $S(Q,\omega)$ arises at frequencies above $\approx 2\pi/0.03$ ps or ≈ 140 meV, much higher than the upper experimentally accessible limit (ω_{max} is 10 meV at $Q = 1.5$ Å^{-1}).

The dynamic structure factor $S(Q,\omega)$ shown in Figure 4 corresponds to the signal observed on a idealized spectrometer having a delta shape instrumental resolution $R(\omega)$. When, for our purposes, the (Q-dependent) function $R(\omega)$ of the NEAT spectrometer is described as a Gaussian plus a very small Lorentzian (see section II), convolution with $S(Q,\omega)$ via the DRT's is direct for the Lorentzian part and requires a simple quadrature for the Gaussian part. We obtained in this way the convoluted function $S^c(Q,\omega)$, i.e., the experimentally accessible dynamic structure factor reconstructed from the simulated hydrogen dynamics, which is shown in Figure 4 together with its unconvoluted version.

IV. Bare Data Comparison between Experiment and Simulation

The experimental incoherent dynamic structure factors of $C_{44}H_{90}$ and PE2K are compared to the results of MD simulations in terms of convoluted $S^c(Q,\omega)$ data in Figure 5a−d for four Q values. To carry out a meaningful comparison between simulated and experimental

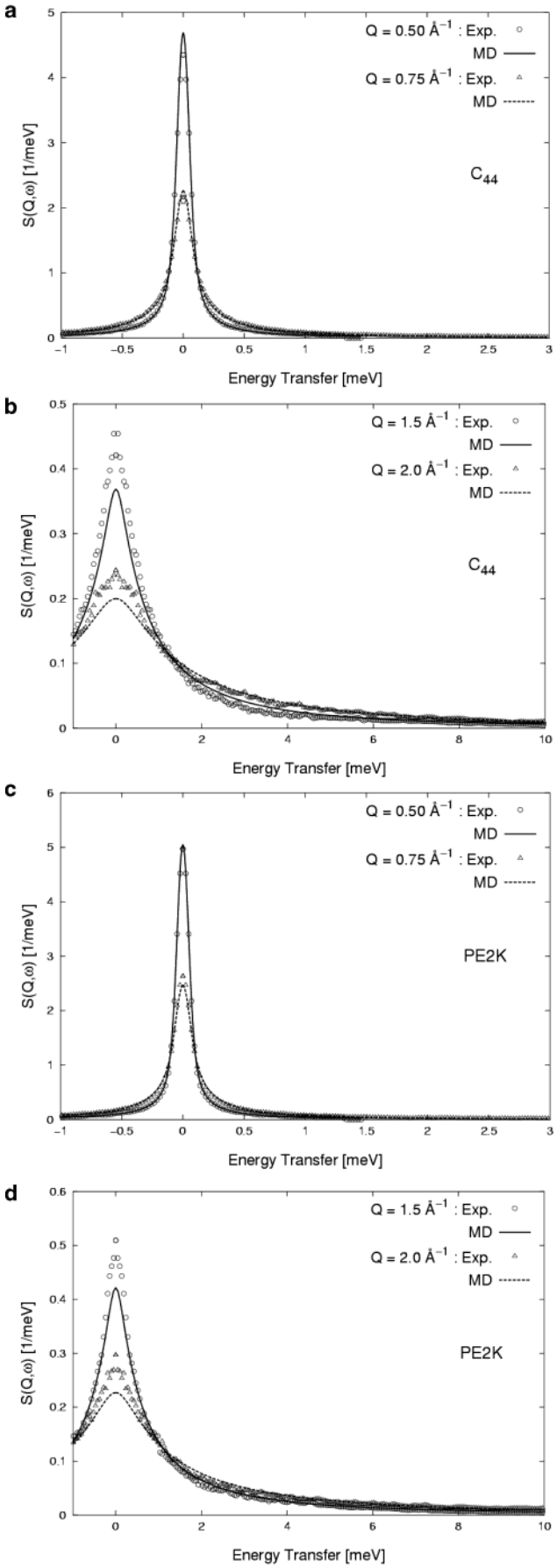

Figure 5. Bare data comparison between experimental (open symbols) and simulation (continuous curves) estimates of $S^{c,norm}(Q,\omega)$ (see eq 6) for four Q values per chain length. (a, b) refer to $C_{44}H_{90}$ and (c, d) refer to PE2K.

$S^c(Q,\omega)$, following Zorn et al.,[38] we have normalized both functions in the same way as

$$S^{c,norm}(Q,\omega) = \frac{S^c(Q,\omega)}{\int_{-\omega_{max}}^{+\omega_{max}} d\omega\ S^c(Q,\omega)} \quad (5)$$

where ω_{max} is the experimental high-frequency limit (i.e., $\Delta E_{max} = 1.4$, 3.5, and 10 meV for $Q = 0.5$, 0.75, and 1.5 Å^{-1}, respectively). This normalization allows us to compare directly the experimental and simulated dynamic structure factors under the constraint that their integral in the experimental window is equal. It eliminates at the same time the influence of the Debye−Waller factor. We stress here once again that, due to the width of instrumental resolution, comparison between experimental and simulated data is limited to the frequency range above $\omega_{min} \approx 0.04$ meV.

Data shown in Figure 5 indicate that the agreement level between experimental measurements and simulated curves is similar for both C_{44} and C_{154}. While there is very good agreement in the quasi-elastic regime at 0.5 and 0.75 Å^{-1}, this agreement is only moderate at higher Q values where the simulated curves are broader indicating faster dynamics. This may be because, in our united atom model where the hydrogen masses are merged with the carbon ones and located at the carbon nuclei, the inertial factors involved in torsion librations are slightly underestimated. At each given Q, both experimental and simulation curves yield effective relaxation times ($S^c(Q,\omega)$ at $\omega = 0$) which are higher for the longer chains. As discussed in section III, the differences should result primarily from the higher mobility of the chain ends, whose concentration is non negligible only for C_{44}.

V. Stretched Exponential and Two-Exponential Representations of the Relaxation Functions

a. General Considerations. Analysis of relaxation processes is often carried out using the empirical Kohlrausch−Williams−Watts (KWW) function or stretched exponential[39]

$$I^{SE}(Q,t) = \exp\left[-\left(\frac{t}{\tau_{KWW}}\right)^{\beta}\right] \quad (6)$$

with $0 < \beta \leq 1$. This function has been extensively used to describe the QENS broadening observed in polymer melts in both time and frequency domains,[38,40−43] and it is therefore of interest to evaluate here to which extent this ad-hoc function describes the quasi-elastic broadening of PE oligomers data in the experimentally accessible Q and ω range. We note that Rennie et al.[18] have analyzed PE data at 447 K in the Q range going from 0.1 to 0.3 Å^{-1} using a single KWW function. In that regime where the diffusion process largely dominates the signal, they found (i) a (Q independent) stretching parameter equal to $\beta = 0.5$, which is indeed close to the value we find for $Q < 1.0$ Å^{-1} (see Table 1), and (ii) a power law exponent $n = 3$ for the Q scaling of τ_{KWW}. Given the rather different Q regime, we can only say that this power law at low Q is consistent with the fast Q dependence of τ_c we observe at higher Q values.

In addition to using a KWW function, the QENS data of polymeric materials have often been analyzed in terms of a sum of two Lorentzians. For polyethylene melts, this approach has already been used by Buchenau et al.,[19] who found that the QENS data, in the temperature range 415−535 K and Q range 0.2−2.2 Å^{-1}, could be fitted by a superposition of two Lorentzians. The two underlying processes were found to have different features. The narrow component was characterized by a Q^2-dependent broadening, indicative of a monomer/segmental free diffusion process. On the converse, the broader component could be fitted equally well by using two different models: (a) restricted diffusion within a sphere or (b) quasi-harmonic vibration. The second model was found to be more realistic and the results consistent with an additional study of drawn deuterated semicrystalline polyethylene at low temperature. A similar procedure was adopted by Kanaya et al.[20] to analyze the QENS data of PE close to 450 K. Using a model consisting of two Lorentzians, these authors were able to describe the PE local dynamics in terms of a fast process on the picosecond time scale and a slower one, called the E process, on a 10 ps time scale. The latter was related to a jump diffusion process which omits the connectivity of the chain.

Table 1. Stretched Exponential Parameters for $I(Q,t)$ Estimated on the Basis of Experimental Data or on the Basis of Simulation Data[a]

N	Q (Å^{-1})	exp/sim	β	τ_{KWW} (ps)	τ_c (ps)	χ
C_{44}	0.5	exp	0.56	9.99	16.6	9×10^{-3}
		sim (conv)	0.54	11.8	20.9	2×10^{-3}
		sim (nonconv)	0.50	11.2	22.4	1×10^{-2}
	0.75	exp	0.56	2.93	4.82	4×10^{-3}
		sim (conv)	0.52	2.83	5.26	4×10^{-3}
		sim (nonconv)	0.49	2.60	5.39	6×10^{-3}
	1.5	exp	0.75	0.68	0.81	2×10^{-3}
		sim (conv)	0.67	0.48	0.64	2×10^{-3}
		sim (nonconv)	0.65	0.46	0.62	1×10^{-3}
	2.0	exp	0.66	0.28	0.37	2×10^{-3}
		sim (conv)	0.70	0.25	0.31	7×10^{-4}
		sim (nonconv)	0.69	0.24	0.31	7×10^{-4}
PE2K	0.5	exp	0.47	13.7	30.5	1×10^{-2}
		sim (conv)	0.52	14.6	27.4	1×10^{-3}
		sim (nonconv)	0.50	14.2	28.5	1×10^{-2}
	0.75	exp	0.48	3.35	7.15	3×10^{-3}
		sim (conv)	0.53	3.41	6.09	4×10^{-3}
		sim (nonconv)	0.50	3.18	6.25	6×10^{-3}
	1.5	exp	0.63	0.62	0.89	3×10^{-3}
		sim (conv)	0.65	0.55	0.74	2×10^{-3}
		sim (nonconv)	0.64	0.52	0.73	1×10^{-3}
	2.0	exp	0.62	0.30	0.43	2×10^{-3}
		sim (conv)	0.67	0.27	0.36	8×10^{-4}
		sim (nonconv)	0.66	0.26	0.35	7×10^{-4}

[a] For the latter, we mention best fit parameters of normalized curves using either the convoluted data $S^{c,norm}(Q,\omega)$ (as defined in eq 5) or the corresponding nonconvoluted $S^{norm}(Q,\omega)$ MD data (see text). τ_c represents the effective relaxation time, namely the area under the KWW curve. The last column characterizes the quality of the $S^{c,norm}(Q,\omega)$ (or $S^{norm}(Q,\omega)$) fit through the corresponding χ value.

b. Fitting PE Data at 450 K. The $S^{c,norm}(Q,\omega)$ data obtained from eq 5 and shown in Figure 5 were fitted using the model function $S^{mod}(Q,\omega)$,

$$S^{mod}(Q,\omega) = \frac{S^{c,SE}(Q,\omega)}{F^{c,SE}(Q,\omega_{max})} \quad (7)$$

where $S^{c,SE}(Q,\omega)$ is the FT of the stretched exponential, convoluted with the resolution function, and $F^{c,SE}(Q,\omega_{max})$ represents its integral over the range $[-\omega_{max},+\omega_{max}]$. Excellent fits were achieved for both C_{44} and PE2K and for both experimental and MD data. This

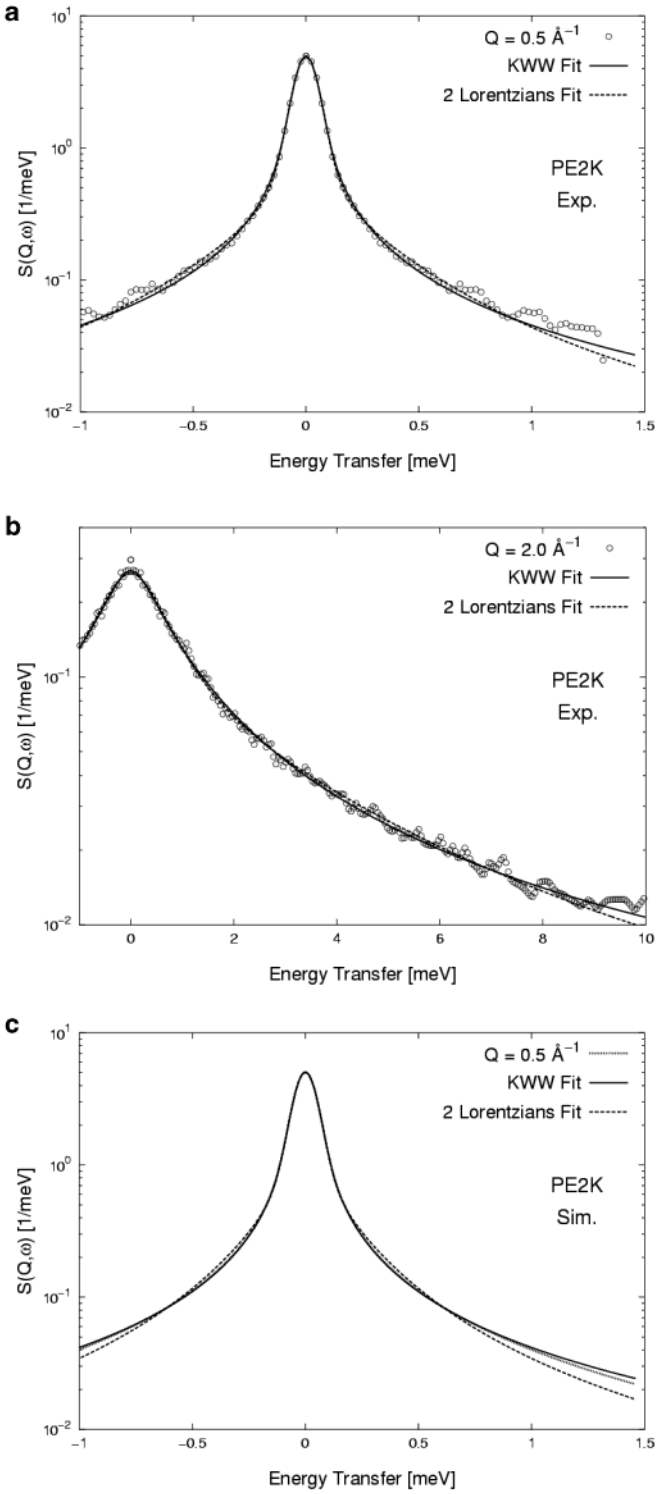

Figure 6. KWW (continuous lines) and two-Lorentzian (dashed lines) fits of $S^{c,norm}(Q,\omega)$ for PE2K (open symbols). (a, b) refer to experiment for $Q = 0.5$ and 2.0 Å^{-1}, respectively, and (c) refer to simulation for $Q = 0.5$ Å^{-1}. Best fit parameters are gathered in Table 1 (KWW) and in Figure 7 (two Lorentzians).

is illustrated in Figure 6a,b for experimental data for the two extreme probed Q values and in Figure 6c for simulation data at $Q = 0.5$ Å^{-1}. All best fit parameters β and τ_{KWW} for $S^{c,norm}(Q,\omega)$ data at 450 K are listed in Table 1, together with the corresponding χ parameter of the fits which represents the square root of the mean-squared deviation. Interestingly, at all Q values, the fit quality was not improved if a faster dynamic process

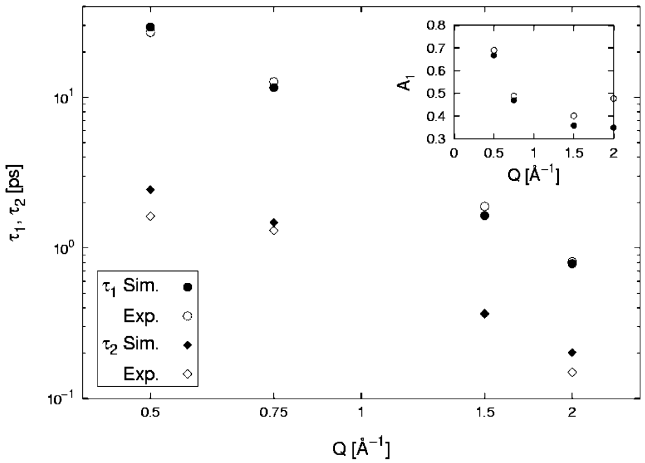

Figure 7. Plot of the relaxation times $\tau_1 = \Gamma_1^{-1}$ and $\tau_2 = \Gamma_2^{-1}$ relative to the two-Lorentzian fits of the $S^{c,norm}(Q,\omega)$ data for PE2K at 450 K, both for experiments (open symbols) and simulations (filled symbols). The inset shows the amplitude of the slow process $A_1(Q)$ vs Q.

occurring outside the experimental range was added to the stretched exponential model in eq 7.

As shown in Table 1, for both chain sizes, the stretched exponent increases with increasing Q. This Q dependence of the β parameter suggests the existence of different elementary dynamic contributions with Q-dependent amplitudes resulting in a progressive change of the shape of the distribution of relaxation times. We will come back to this point in section VI where a more elaborate analysis of the MD data is developed.

We list also in the table the effective relaxation time $\tau_c = \tau_{KWW}\Gamma(1/\beta)/\beta$ corresponding to the area under the stretched exponential decay. At the lowest Q value, the effective relaxation time for the C_{44} oligomer is almost half the value obtained for PE2K. This difference decreases with increasing Q. This result could be interpreted as the signature of a chain end effect through an enhancement of the monomeric diffusion in space, a process which is better seen in the lower Q range.

To be able to compare our MD and experimental data with results published in the literature, we have fitted the convoluted $S^{c,norm}(Q,\omega)$ curves where the stretched exponential model function in eq 7 is replaced by a sum of two Lorentzians with three parameters, namely the widths Γ_1 and Γ_2 and the amplitude A_1 of the slowest process.

In Figure 7, we plot the fit parameters obtained from both experimental and simulated PE2K data (a similar trend was observed for C_{44}). Data show that there is reasonably good agreement between experimental and simulation fit parameters at all Q's. In particular, the fast process is characterized by a relaxation time $\tau_2(Q)$ (inverse of Γ_2) in the picosecond range which decreases with Q increasing, in agreement with previous experiments.[19] The slowest process relaxation time has a more pronounced Q dependence which does not seem to follow a power law. The amplitude of the slow process decreases as Q increases except when Q reaches 2 Å^{-1} in the experimental case only. We think that this anomaly is related to the fact that the two-exponential relaxation model loses meaning for Q above 1.5 Å^{-1} as both relaxation times get too close and τ_2 becomes smaller than t_{min}, that is the shortest time probed by the spectrometer.

Regarding the corresponding fit quality with respect to what was found for the stretched exponential model, we observe for the experimental data a rather similar agreement level for both models, as is illustrated in Figure 6a,b. Figure 6c shows that at low Q the stretched exponential model appears even superior for reproducing the simulation data. This is confirmed by comparing the χ values found for stretched exponential fits (see Table 1) to the ones associated with the two-Lorentzian model which are around 7×10^{-3} for $Q = 0.5$ and 0.75 Å^{-1} and around 1×10^{-3} for $Q = 1.5$ and 2.0 Å^{-1}, for both the simulated and experimental data.

On this basis, we conclude that a two-Lorentzian model (three free parameters per Q value) is not better than a stretched exponential (two free parameters) in describing the QENS data for polyethylene. Therefore, the time-of-flight data do not give any indication on the existence of two distinct dynamic processes, nor in the time, nor in the frequency domain. This is not the case for most polymers where the local dynamics relaxation is clearly split into a fast process in the picosecond range and a much slower process.[21−24]

While the Q dependence of the stretched exponent and the reasonable fits in terms of two Lorentzians suggest that the local dynamics of PE, in the time-of-flight frequency range, could be rationalized in terms of two distinct processes, there appears to be no clear evidence for this neither in the QENS nor in MD $S^c(Q,\omega)$ data. This is in contrast with most amorphous polymers for which the presence of two distinct processes is very clear.[21−24] In the next section, we will exploit the distribution of relaxation times obtained at 450 K from the simulated relaxation functions at different Q's to appreciate, without the bias of a particular model function, to which extent they reveal either a single broad process or two separate processes.

VI. A DRT Analysis of the Simulated Local Dynamics Relaxation Functions for Long Chains

So far, we have treated experimental and simulation data on an equal footing and applied empirical functions to analyze the corresponding $S(Q,\omega)$ curves. This has made it possible to compare our MD and experimental data and provide links with published reports.

In the probed Q range, all simulated curves decay monotonically to zero within the accessible simulation time window (see Figure 2), which is considerably larger than the 0.4−20 ps time window which has been exploited so far on the basis of the convoluted signal $S^{c,norm}(Q,\omega)$ defined in eq 5. To exploit the whole information available from MD and go beyond data interpretation in terms of empirical functions with few parameters, we have performed a detailed analysis of the bare $I_{core}(Q,t)$ function (which is practically equivalent to the $I(Q,t)$ data of PE2K) at 450 K.

As mentioned earlier, the knowledge of the full decay of correlation functions makes it numerically feasible to extract $F(\ln \tau)$, the normalized distribution of relaxation times (DRT)[44,9,35] defined in eq 3, by a CONTIN[36,37] analysis. The DRT functions obtained by this procedure are shown in Figure 8 for all investigated Q values, and the corresponding fits are shown in Figure 2. Numerical details on the CONTIN procedure, as applied in the present context, are gathered in the Appendix.

It is shown in Figure 8 that the shape of the DRT functions changes with Q. At high Q values, the curves

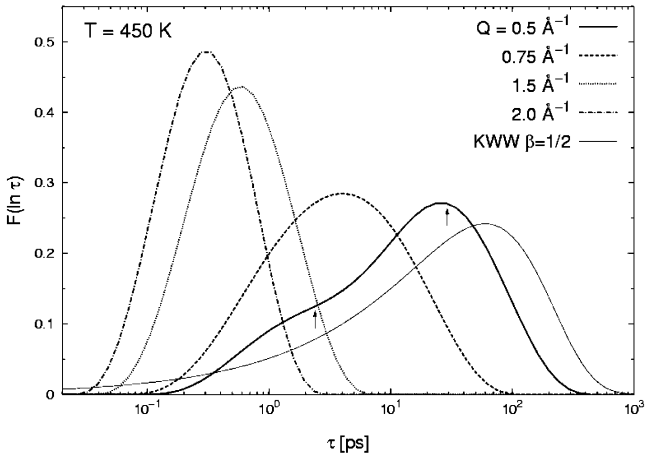

Figure 8. Distribution of relaxation times $F(\ln \tau; Q)$ relative to the incoherent intermediate structure factor $I_{core}(Q,t)$ at 450 K computed by MD simulations for $Q = 0.5$, 0.75, 1.5, and 2 Å^{-1} (see also Figure 2). For comparison, the DRT of a KWW function with $\beta = 0.5$ and arbitrary relaxation time is plotted (thin lines) on the right-hand side. The arrows indicate the two relaxation times found when fitting the dynamic structure factor at $Q = 0.5$ Å^{-1} with the two-Lorentzian model (see text).

are symmetric and can be represented by a log−Gaussian distribution of τ. As Q decreases, the distribution broadens and becomes increasingly asymmetric, although it does not attain the level of asymmetry expected for $\beta = 0.5$, a representative value of the stretched exponent found for PE2K or C_{44} relaxation at $Q \leq 0.75$ Å^{-1} (see Table 1). This is evident in Figure 8 where the DRT corresponding to a KWW function with $\beta = 0.5$ is plotted for comparison. Finally and quite interestingly, at the lowest Q investigated, i.e., 0.5 Å^{-1}, two processes can be clearly resolved.

Actually, stretched exponential functions are indicative of nonexponential processes with a distribution of relaxation times whose asymmetry increases as β decreases from 1 to 0. In section V, on the basis of the convoluted signal $S^c(Q,\omega)$, we have noted that the stretched exponent increases from ca. $\beta = 0.5$ at $Q = 0.5$ Å^{-1} toward values approaching unity as Q increases. This systematic evolution of the stretching exponent with Q is coherent with the evolution in the shape of the distribution of relaxation times. Thus, the KWW function is able to capture some of the general features of the DRT analysis, namely the evolution of the distributions toward narrower and increasingly more symmetric functions with increasing Q (see Figure 8). However, we note that the distributions corresponding to $Q \geq 1$ Å^{-1} are much closer to a log−normal distribution than to any stretched exponential, the latter being always too unsymmetrical.

In section V, we have discussed the stretched exponential fitting, independently for each Q, of the convoluted function $S^c(Q,\omega)$ generated by MD (see Table 1 and Figure 6c). We can repeat the procedure over a much larger frequency range, using eqs 5−7 with the unconvoluted simulated signal directly obtained using eq 4. The test of the stretched exponential model function over a much larger frequency window leads, as we observe in Table 1, to minor changes in the optimal parameters and in the fit overall quality except at $Q = 0.5$ Å^{-1} where parameters do change significantly and where the fit quality turns out to be worse with typical deviations being increased by 1 order of magni-

tude. So, in conclusion, despite its numerical applicability in the experimental frequency range, the single stretched exponential model treats effectively a mixture of two processes in an ad-hoc way, and the link with physical parameters characterizing the two processes is impossible.

Obviously, the distributions shown in Figure 8 do not resemble the two delta functions distribution that would be expected on the basis of a two-Lorentzian model which was also studied in section V. We observe that the two relaxation times and the amplitude at $Q = 0.5$ Å^{-1} and 450 K ($\tau_1 = 29.2$ ps, $\tau_2 = 2.4$ ps, $A_1 = 0.67$; see also Figure 7) do correspond (see vertical arrows at times τ_1 and τ_2 in Figure 8) to the main peak position and the shoulder of the DRT. To evaluate amplitudes and mean relaxation times, it is necessary to decompose numerically the DRT into the sum of two distributions, each corresponding to a single process. No simple quantitative partitioning of the DRT into two elementary distributions is provided by the CONTIN procedure because the latter separates peaks at minima positions (see Appendix) while the possible coexistence of two distinct relaxation processes is only suggested by a shoulder at the lowest Q value. One can tentatively perform an ad-hoc decomposition by assuming that the distribution is the superposition of two symmetric distributions in ln τ. On this basis, we get an amplitude of 0.72 ± 0.07 for the slow process, which is coherent with the amplitude of 0.67 found for the slowest process in the double-exponential model (see inset in Figure 7). For $Q > 0.5$ Å^{-1} we observe that the two relaxation times provided by the two Lorentzians fit reported in Figure 7 are such that the difference between ln τ_1 and ln τ_2 merely represents the width of the unimodal $F(\ln \tau)$ distribution (see Figure 8).

A question arises: how can we explain the fact that at 450 K, the PE local dynamics relaxation proceeds via a mixed process involving torsional oscillations and conformational jumps while both types of motion lead generally in other polymers to a clear-cut time scale separation?[21−24] One possible explanation is that the temperature range where linear PE is in a melt state corresponds to temperatures that are unusually high with respect to the glass transition of roughly 150 K in PE[45] (estimated in the homogeneous amorphous phase without interferences with confinement effects due to partial crystallization). An alternative explanation is that torsional motions and jumps are highly cooperative and fast in molten PE because, in the absence of side groups, these motions are not necessarily coupled to flow relaxation,[4] and this may contribute to produce a single peak distribution of relaxation times.

To check unambiguously the existence of two processes and to fully characterize them, we need to extend the analysis toward lower Q values or lower temperatures. Reference 25 reports a simulation study of the PE model system used in the present paper at a much lower temperature of 350 K (undercooled liquid). The analysis (see Figure 2 of ref 25) shows a double peak in the DRT function for the whole Q regime going from 0.5 to 2 Å^{-1} explored in the present paper, suggesting a stronger temperature dependence of the slower process. While the position of the peak associated with the fastest process is slightly Q-dependent, its amplitude increases from roughly 15% at $Q = 0.5$ Å^{-1} to about 90% at $Q = 2$ Å^{-1}. On the contrary, the slowest process appears to be strongly Q-dependent. The fastest process (occurring on a time scale of 0.5−1 ps) has been shown to be a very localized process related to the vibration−torsion oscillations of the polymer backbone. The slowest one must be a diffusive process resulting from a succession of conformational changes over the rotational barriers. This picture has already been suggested earlier in experimental works[19,20] and tested in simulations of PE at 504 K, using artificially high rotational barriers.[12]

VII. Conclusions

In this paper, we provide new experimental data on the incoherent dynamic structure factor of two PE oligomers, C_{44} and PE2K (or C_{154}), at 450 K. The QENS experimental data and in particular the trend observed with increasing chain length are reproduced by MD. The experimental and MD incoherent dynamic structure factors were analyzed using different models in order to provide a direct link between our results and published data.

It has been already suggested that, for PE, two dynamic processes are active in the QENS frequency range. The problems associated with isolating and characterizing these two processes have been discussed in detail in this work. The DRT analysis of the core dynamics of PE at 450 K shows, in the Q range probing local dynamics, that the two processes occur on similar time scales at this temperature.

Our simulations on a large time window (10 ns) indicate that at 350 K there is an unambiguous evidence of two distinct processes.[25] PE is a semicrystalline polymer with relatively high melting temperature ($T_m \approx 400$ K); this precludes experiments at 350 K, but nevertheless we are presently performing experiments on PE oligomers with lower T_m in order to probe the local dynamics at the lowest accessible temperature for the melt.

Because of the high temperatures examined in experiments and the limited frequency ranges, data can be satisfactorily fitted using both the Fourier transform of the stretched exponential function or two Lorentzians. Ideally, a full DRT analysis of the experimental data on melts at $T \approx 400$ K should be conducted as this leads to model-free results (other than assuming that the analyzed processes are not inherently nonexponential and that the inverse Laplace transform of the correlation function exists). This requires precise data on a wide frequency window which can be only obtained by combining information from instruments with different energy resolutions. Overlapping $S(Q,\omega)$ data from TOF and backscattering spectrometers covering a sufficiently large energy window is also the target of our present experimental efforts.

Finally we wish to highlight the power of combined simulation/experimental data treatments. In the present paper, we have suggested that normalized $S^{c,norm}(Q,\omega)$ functions in the experimental accessible energy window are ideal to bridge experimental data to MD simulations, provided the latter are accurate enough to perform safely the numerical operations (FT and convolution with the experimental resolution function of low noise input $I(Q,t)$ functions). Comparison efforts along these lines are also done in connection with NMR data on PE.[4]

Acknowledgment. We thank Georges Destrée for invaluable help in the numerical analysis. G. Arialdi

acknowledges financial support (PhD grant) from the Fonds pour la formation à la Recherche dans l'Industrie et dans l'Agriculture (FRIA) de la Communauté française de Belgique. Support from Directorate General 12 of the European Commission in the context of the TMR Research Training Network "New Routes to Understanding Polymers Using Experiments and Realistic Modelling" (NEWRUP), Contract No. ERB-FMRX-CT98-0176, is gratefully acknowledged. We thank BENSC for beam time and the EU for financial support through the Human Potential Programme under IHP-ARI Contract HPRI-CT-1999-00020.

Appendix

A monotonically decreasing correlation function $C(t)$ between $t = 0$ and $t = \infty$ can be written in terms of a continuous linear combination of decaying exponentials

$$C(t) = \int_{-\infty}^{+\infty} \mathrm{d}\ln\tau\, F(\ln\tau)\exp(-t/\tau) \qquad \text{(A1)}$$

where the weight $F(\ln\tau)$ (normalized in the logarithmic scale) is known as the distribution of relaxation times (DRT).[9,35−37] Equation A1 shows that the $F(\ln\tau)$ function is the inverse Laplace transform of the observed time correlation function.

In the present context, $C(t)$ is the intermediate scattering function $I(Q,t)$. Since $I(Q,t{=}0) = 1$, the $F(\ln\tau; Q)$ functions corresponding to the DRT are automatically normalized to 1. It is useful to realize that the $F(\ln\tau; Q)$ function can be used to express the average (global) relaxation time $\langle\tau\rangle$ as

$$\int_0^{+\infty} I(Q,t)\,\mathrm{d}t = \int_{-\infty}^{+\infty} \mathrm{d}\ln\tau\, F(\ln\tau;Q)\int_0^{+\infty} \mathrm{d}t\, \mathrm{e}^{-t/\tau} = \int_{-\infty}^{+\infty} \tau F(\ln\tau;Q)\,\mathrm{d}\ln\tau \equiv \langle\tau\rangle \qquad \text{(A2)}$$

hence its denomination as the "distribution of relaxation times function".

In our context, the input information for the CONTIN numerical procedure[36,37] consists of the relaxation function itself (in this case the $I(Q,t)$ data), of the lower and the upper limit in which the distribution of relaxation times is expected to be found, of the required number of points in τ (equidistant in the logarithmic scale), and finally of a rather flexible option for which the author's suggestion of 10−12 points per decade was followed.[36,37] Limiting values can be specified so that the distribution vanishes before reaching them. The program furnishes a set of solutions (in our case about 10) for the DRT. Each solution is characterized by (i) a "regularization parameter" α which gives a measure of the smoothness of the DRT and (ii) a measure of the fit quality specified by a mean-squared deviation. The analysis for correlation functions characterizing polymer local dynamics usually results only to few solutions (typically one or two for correlation functions with a time resolution similar to the one adopted here) which simultaneously possess the minimum number of peaks (the number of peaks is one or two, exceptionally three[35,46]) and can provide a satisfactory fit of the simulation data. In case that more than one solution satisfies these criteria, we have always adopted the "physical" solution on the basis of the parsimony principle, which dictates that the less detailed spectrum which gives a reasonable fit to the data must be selected.

Within the DRT approach, if $F(\ln\tau)$ presents several peaks, then the amplitude A_i and characteristic time $\langle\tau_i\rangle$ of each peak are

$$F(\ln\tau) = \sum_i F_i(\ln\tau) \qquad \text{(A3)}$$

with

$$A_i = \int_{-\infty}^{+\infty} F_i(\ln\tau)\,\mathrm{d}\ln\tau \qquad \text{(A4)}$$

and

$$\langle\tau_i\rangle = \frac{1}{A_i}\int_{-\infty}^{+\infty} \tau F_i(\ln\tau)\,\mathrm{d}\ln\tau \qquad \text{(A5)}$$

These definitions imply the normalization $\sum_i A_i = 1$ and a link between the average times of individual processes and the global relaxation time, namely $\langle\tau\rangle = \sum_i A_i\langle\tau_i\rangle$.

References and Notes

(1) Mendelson, R. A.; Bowles, W. A.; Finger, F. L. *J. Polym. Sci., Part A-2* **1970**, *8*, 105.
(2) Raju, V. R.; Smith, G. G.; Marin, G.; Knox, J. R.; Graessley, W. W. *J. Polym. Sci., Polym. Phys. Ed.* **1979**, *17*, 1183.
(3) McKenna, G. B.; Ngai, K. L.; Plazek, D. J. *Polymer* **1985**, *26*, 1651.
(4) Qiu, X. H.; Ediger, M. D. *Macromolecules* **2000**, *33*, 490.
(5) Roe, R.-J. *J. Chem. Phys.* **1994**, *100*, 1610.
(6) Brown, D.; Clarke, J. H. R.; Okuda, M.; Yamazaki, T. *J. Chem. Phys.* **1994**, *100*, 1684.
(7) Boyd, R. H.; Gee, R. H.; Han, J.; Jin, Y. *J. Chem. Phys.* **1994**, *101*, 788.
(8) Harmandaris, V. A.; Mavrantzas, V. G.; Theodorou, D. N. *Macromolecules* **1998**, *31*, 7934.
(9) Karatasos, K.; Adolf, D. B.; Hotston, S. *J. Chem. Phys.* **2000**, *112*, 8695.
(10) Smith, G. D.; Yoon, D. Y.; Zhu, W.; Ediger, M. D. *Macromolecules* **1994**, *27*, 5563.
(11) Paul, W.; Smith, G. D.; Yoon, D. Y. *Macromolecules* **1997**, *30*, 7772.
(12) Smith, G. D.; Paul, W.; Yoon, D. Y.; Zirkel, A.; Hendricks, J.; Richter, D.; Schober, H. *J. Chem. Phys.* **1997**, *107*, 4751.
(13) Paul, W.; Smith, G. D.; Yoon, D. Y.; Farago, B.; Rathgeber, S.; Zirkel, A.; Willner, L.; Richter, D. *Phys. Rev. Lett.* **1998**, *80*, 2346.
(14) Peterlin-Neumaier, T.; Springer, T. *J. Polym. Sci., Polym. Phys. Ed.* **1976**, *14*, 1351.
(15) Hohlweg, G.; Holzer, B.; Petry, W.; Strobl, G.; Stühn, B. *Macromolecules* **1992**, *25*, 6248.
(16) Holzer, B.; Strobl, G.; Stühn, B.; Andersen, N. H. *Colloid Polym. Sci.* **1994**, *272*, 1396.
(17) Kanaya, T.; Buchenau, U.; Koizumi, S.; Tsukushi, I.; Kaji, K. *Phys. Rev. B* **2000**, *61*, R6451.
(18) Rennie, A. R.; Petry, W.; Stühn, B. In *Polymer Motion in Dense Systems*; Richter, D., Springer, T., Eds.; Springer Proceedings in Physics 29; Springer: Heidelberg, 1988; p 235.
(19) Buchenau, U.; Monkenbusch, M.; Stamm, M.; Majkrzak, C. F.; Nücker, N. In *Polymer Motion in Dense Systems*; Richter, D., Springer, T., Eds.; Springer Proceedings in Physics 29; Springer: Heidelberg, 1988; p 138.
(20) Kanaya, T.; Kawaguchi, T.; Kaji, K. *Macromolecules* **1999**, *32*, 1672.
(21) Colmenero, J.; Alvarez, F.; Arbe, A. *Phys. Rev. E* **2002**, *65*, 041804.
(22) Colmenero, J.; Arbe, A.; Coddens, G.; Frick, B.; Mijangos, C.; Reinecke, H. *Phys. Rev. Lett.* **1997**, *78*, 1928.
(23) Zorn, R.; Arbe, A.; Colmenero, J.; Frick, B.; Richter, D.; Buchenau, U. *Phys. Rev. E* **1995**, *52*, 781.
(24) Ahumada, O.; Theodorou, D. N.; Triolo, A.; Arrighi, V.; Karatasos, K.; Ryckaert, J.-P. *Macromolecules* **2002**, *35*, 7110.
(25) Arialdi, G.; Ryckaert, J.-P.; Theodorou, D. N. *Chem. Phys.* **2003**, *292*, 371.
(26) Lechner, R. E.; Melzer, R.; Fitter, J. *Physica B* **1996**, *226*, 86 and refs 2 and 3 given therein.
(27) See: http://www.ill.fr/tof/TOFHR_software/INGRID.html.
(28) Ryckaert, J.-P.; Bellemans, A. *Chem. Phys. Lett.* **1975**, *30*, 123.

(29) Pant, P. V. K.; Theodorou, D. N. *Macromolecules* **1995**, *28*, 7224.
(30) Mavrantzas, V. G.; Boone, T. D.; Zervopoulou, E.; Theodorou, D. N. *Macromolecules* **1999**, *32*, 5072.
(31) Pearson, D. S.; Ver Strate, G.; von Meerwall, E.; Schilling, F. C. *Macromolecules* **1987**, *20*, 1133.
(32) Gō, N.; Scheraga, H. A. *Macromolecules* **1976**, *9*, 535.
(33) van Gunsteren, W. F. *Mol. Phys.* **1980**, *40*, 1015.
(34) Destrée, M.; Lauprêtre, F.; Lyulin, A.; Ryckaert, J.-P. *J. Chem. Phys.* **2000**, *112*, 9632.
(35) Karatasos, K.; Ryckaert, J.-P. *Macromolecules* **2001**, *34*, 7232.
(36) Provencher, S. W. *Comput. Phys. Commun.* **1982**, *27*, 213.
(37) Provencher, S. W. *EMBL Technical Report DA07*; European Molecular Biology Laboratory: Heidelberg, 1984.
(38) Zorn, R.; Kanaya, T.; Kawaguchi, T.; Richter, D.; Kaji, K. *J. Chem. Phys.* **1996**, *105*, 1189.
(39) Williams, G.; Watts, D. C. *Trans. Faraday Soc.* **1970**, *66*, 80.
(40) Ngai, K. L.; Colmenero, J.; Alegría, A.; Arbe, A. *Macromolecules* **1992**, *25*, 6727.
(41) Richter, D.; Monkenbusch, M.; Arbe, A.; Colmenero, J.; Farago, B.; Faust, R. *J. Phys.: Condens. Matter* **1999**, *11*, A297.
(42) Arrighi, V.; Ferguson, R.; Lechner, R. E.; Telling, M.; Triolo, A. *Physica B* **2001**, *301*, 35.
(43) Ganazzoli, F.; Raffaini, G.; Arrighi, V. *Phys. Chem. Chem. Phys.* **2002**, *4*, 3734.
(44) Alvarez, F.; Alegría, A.; Colmenero, J. *J. Chem. Phys.* **1995**, *103*, 798.
(45) Rodriguez, F. *Principles of Polymer Systems*, 4th ed.; Taylor & Francis: Washington, 1996.
(46) Triolo, A.; Lechner, R. E.; Desmedt, A.; Telling, M. T. F.; Arrighi, V. *Macromolecules* **2002**, *35*, 7039.

MA0256789